Available online at www.sciencedirect.com
SCIENCE DIRECT®
International Journal of Heat and Fluid Flow 26 (2005) 71–79
International Journal of HEAT AND FLUID FLOW
www.elsevier.com/locate/ijhff

Viscous and unsteady flow calculations of condensing steam in nozzles

D.A. Simpson, A.J. White *

Hopkinson Laboratory, Cambridge University Engineering Department, Trumpington Street, Cambridge, CB2 1PZ, UK

Received 12 September 2003; accepted 1 April 2004
Available online 7 June 2004

Abstract

The paper presents two-dimensional calculations for spontaneously nucleating flows of steam in converging–diverging nozzles. The Reynolds-averaged Navier–Stokes equations are solved for the two-phase mixture, using a Jameson-style finite volume method on an unstructured and adaptive triangular mesh. Results are first presented for steady, viscous flow, showing the influence of boundary layer growth on streamwise pressure distributions and droplet sizes. These results have implications for the interpretation of some of the experimental data used for validating the theories of nucleation and droplet growth. The numerical scheme has also been applied to compute unsteady flows in a variety of nozzle geometries, covering a range of inlet conditions in each case. Asymmetric oscillation modes, previously observed in moist air, have been predicted for one of the geometries, indicating for the first time that such oscillations are possible in pure steam.

Keywords: Condensation; Wet-steam; Asymmetric oscillations; Unstructured mesh

1. Introduction

The use of converging–diverging nozzles as a means of studying condensation in steam dates back to the early experiments of Stodola (1905). In such experiments, steam is expanded from an initially saturated or slightly superheated state, and typically acquires sufficient subcooling for spontaneous nucleation of droplets in the diverging section of the nozzle, where the flow is supersonic. The subsequent release of latent heat from growing droplets thus results in a deceleration of the flow and a rise in pressure, known traditionally as the "condensation shock". Measurements of nozzle pressure distributions (e.g., Binnie and Woods, 1938) and, more recently, the use of light scattering data to infer droplet sizes (e.g., Moore et al., 1973) have been used extensively to test the theories of nucleation and droplet growth. Furthermore, nozzle experiments, using both pure steam and moist air, have revealed a variety of interesting phenomena which stem from the coupling between the condensation process and the gas dynamics. These include the formation of true, aerodynamic shock waves when the heat release is supercritical (i.e., more than sufficient to revert the flow to sonic conditions), and oscillatory flow regimes which arise from interaction between such shock waves and the zone of intense nucleation. Recently, an interesting asymmetric oscillation mode has been detected in moist air nozzle flows by Adam and Schnerr (1997), using both experimental and numerical techniques. Phenomena of this sort serve to highlight the dramatic ways in which condensation impacts upon the flowfield, and have implications for practical condensing flows, such as those occurring in low pressure steam turbines.

In the current paper, a two-dimensional calculation method for viscous, wet-steam flow is described. The method employs unstructured, adaptive mesh and is, therefore, able to focus on regions of rapid flow change. Results are presented for both steady and unsteady condensation in nozzles. The steady flow calculations serve to validate the method and also highlight the

* Corresponding author. Tel.: +44-1223-765-310; fax: +44-1223-330-282.
E-mail address: ajw36@cam.ac.uk (A.J. White).

0142-727X/$ - see front matter © 2004 Elsevier Inc. All rights reserved.
doi:10.1016/j.ijheatfluidflow.2004.04.002

Nomenclature

C_μ, C_ϵ	turbulence modelling constants (see Appendix A)
e	specific internal energy
E	total specific internal energy
f_μ	turbulence damping parameter defined by Eq. (A.1)
G	droplet growth rate, $\mathrm{d}r/\mathrm{d}t$
h	specific enthalpy
H	total specific enthalpy
J	nucleation rate per unit mass of mixture
k	turbulent kinetic energy, Boltzmann's constant
l_v	mean free path of vapour molecules
M	mass of H_2O molecule
p	pressure
Pr	Prandtl number of the vapour
q_j	heat flux in jth coordinate direction
R_v	gas constant for H_2O per unit mass
r	droplet radius
r_*	Kelvin–Helmholtz critical radius
t	time
T	temperature, period of oscillation
u_i, u_j	velocity components
v	specific volume
x_i, x_j	spatial coordinates
y	wetness fraction
δ_{ij}	Kronecker delta
ΔT	vapour subcooling, $(T_\mathrm{s} - T_\mathrm{v})$
λ	thermal conductivity of the vapour
μ	dynamic viscosity of the vapour
μ_m	mth order moment of the droplet size distribution
ν	semi-empirical droplet growth parameter (see Young, 1982)
ρ	density
σ	surface tension
τ_{ij}	shear stress
ξ	nucleation rate adjustment, defined by Eq. (B.4)

Subscripts

i, j	coordinate direction indices
l, v	liquid/vapour phase
L, T	laminar/turbulent quantities
m	moment index
s	saturation quantity
01	inlet stagnation state

Unsubscripted quantities refer to mixture values where appropriate.

implications of boundary layer growth for the interpretation of droplet size and pressure measurements. The focus is on how the boundary layer modifies the effective nozzle geometry—other effects, such as the impact of viscous dissipation on nucleation and the droplet size distribution, have been discussed elsewhere (White, 2000). The unsteady results, to the best of the authors' knowledge, constitute the first predictions of asymmetric oscillations for pure steam.

2. Governing equations

The two-phase wet-steam mixture comprises vapour at pressure p and temperature T_v, and spherical liquid droplets at temperature T_l. In general, droplets exist with a continuous distribution of sizes, but are assumed sufficiently small that they travel with the vapour velocity. The liquid temperature is strictly a function of droplet size, but except in the case of extremely small droplets (which make a negligible contribution to the mass of liquid), T_l lies very close to the local saturation temperature, $T_\mathrm{s}(p)$. Thus, with negligible error, mixture specific quantities, such as the specific enthalpy, h, may be written in the form

$$h = (1-y)h_\mathrm{v} + yh_\mathrm{l}, \tag{1}$$

where y is the mass fraction of liquid (the *wetness fraction*), h_v is the specific enthalpy of the vapour, and h_l is the specific enthalpy of saturated liquid evaluated at $T_\mathrm{s}(p)$. Expressions similar to Eq. (1) apply to the mixture specific internal energy, e, and mixture specific volume, v. The mixture density is then given as $\rho = 1/v$.

2.1. Conservation equations

In the absence of velocity slip, the Reynolds-averaged continuity, Navier–Stokes and energy equations for the mixture as a whole take their usual (single-phase) form:

$$\frac{\partial}{\partial t}\begin{pmatrix}\rho\\ \rho u_i\\ \rho E\end{pmatrix} + \frac{\partial}{\partial x_j}\begin{pmatrix}\rho u_j\\ \rho u_i u_j + p\delta_{ij}\\ \rho H u_j\end{pmatrix} = \begin{pmatrix}0\\ \frac{\partial \tau_{ij}}{\partial x_j}\\ \frac{\partial}{\partial x_j}(u_i\tau_{ij} - q_j)\end{pmatrix} \tag{2}$$

where the symbols have their usual meanings, and are given explicitly in the notation or defined below. (All variables are considered as averaged quantities, with densities and pressures taken as time averages, and velocities, internal energy and enthalpy as density-weighted averages.)

2.2. Turbulence modelling

In the Reynolds-averaged form of Eq. (2), the stress tensor components, τ_{ij}, comprise laminar and turbulent contributions which are computed here by means of laminar and turbulent viscosities, μ_L and μ_T, respectively. (Note that the direct effect of turbulent fluctuations on the nucleation rate has not been modelled here.) Thus,

$$\tau_{ij} = (\mu_L + \mu_T)\left(\frac{\partial u_i}{\partial x_j} + \frac{\partial u_i}{\partial x_j} - \frac{2}{3}\frac{\partial u_j}{\partial x_j}\delta_{ij}\right) - \frac{2}{3}\rho k\delta_{ij} \tag{3}$$

where k is the (density-weighted) turbulent kinetic energy.

For the majority of wet-steam flows of practical interest, the volume fraction of the liquid phase is of the order of 10^{-5}. It is thus assumed that the laminar viscosity, μ_L, is given sufficiently accurately by its vapour-phase value. The turbulent viscosity, μ_T, is obtained from a standard k–ε model (Yang and Shih, 1993):

$$\mu_T = \rho f_\mu C_\mu k t_T, \tag{4}$$

which requires solution of transport equations for the turbulent kinetic energy, k, and dissipation rate, ε:

$$\frac{\partial}{\partial t}(\rho k) + \frac{\partial}{\partial x_j}(\rho u_j k) = \frac{\partial}{\partial x_j}\left(\mu_k \frac{\partial k}{\partial x_j}\right) + \tau_{Tij}\frac{\partial u_i}{\partial x_j} - \rho\varepsilon \tag{5}$$

$$\frac{\partial}{\partial t}(\rho\varepsilon) + \frac{\partial}{\partial x_j}(\rho u_j \varepsilon) = \frac{\partial}{\partial x_j}\left(\mu_\varepsilon \frac{\partial \varepsilon}{\partial x_j}\right) + \left(C_{\varepsilon 1}\tau_{Tij}\frac{\partial u_i}{\partial x_j} - C_{\varepsilon 2}\rho\varepsilon\right)\frac{1}{t_T}, \tag{6}$$

where $\mu_k = \mu_L + \mu_T/\sigma_k$ and $\mu_\varepsilon = \mu_L + \mu_T/\sigma_\varepsilon$. Details of the various parameters and constants used in the turbulence model are given in Appendix A. Heat fluxes, q_j, (see Eq. (2)) also comprise laminar and turbulent components, and hence are given by:

$$q_j = -(\lambda_L + \lambda_T)\frac{\partial T_v}{\partial x_j}, \tag{7}$$

where the turbulent thermal conductivity, λ_T, is determined by specifying a turbulent Prandtl number of 0.9.

2.3. Growth of the liquid phase

Closure of the conservation equations requires computation of the wetness fraction, y, which changes by virtue of nucleation and droplet growth. For the calculations presented here, the polydispersed nature of the droplet size distribution is treated by means of a moment-based method, first introduced by Hill (1966). A full description of this method applied to wet-steam flow is given by White and Hounslow (2000). Defining the size distribution, $f(r)$, such that $f(r)\mathrm{d}r$ is the number of droplets per unit mass of mixture in the size range r to $r + \mathrm{d}r$, the wetness fraction is given by,

$$y = \frac{4}{3}\pi\rho_l \int_0^\infty f(r) r^3 \mathrm{d}r = \frac{4}{3}\pi\rho_l \mu_3 \tag{8}$$

where μ_3 is the third moment of the size distribution. This (and other lower-order moments) is computed from the general evolution equation for the m-th moment, μ_m:

$$\frac{\partial}{\partial t}(\rho\mu_m) + \frac{\partial}{\partial x_j}(\rho\mu_m u_j) = m\rho\overline{G}\mu_{m-1} + \rho J r_*^m, \quad m = 0, 1, 2, 3 \tag{9}$$

where J and r_* are the nucleation rate and critical radius, respectively, and $\overline{G}$ is the growth rate averaged for the entire distribution of droplet sizes. Expressions for J, r_* and $\overline{G}$ are given in Appendix B.

3. Numerical implementation

The numerical scheme employed here is a two-dimensional version of an unstructured tetrahedral flow solver developed by Dawes (1992). The equations of motion (2), (5), (6) and moment equation (9) are discretised in finite volume form on triangular cells (Fig. 1) using cell-vertex storage. The equations are applied to a control volume composed of the cells surrounding each node, as shown by the shaded region in the figure. Convective fluxes across each of the cell interfaces are first computed by averaging quantities at the two delimiting nodes. The central node, K, thus receives flux contributions from each of the interfaces forming the perimeter of the control volume. Viscous and other dissipative terms are treated as source terms and are determined by repeated application of the Gauss divergence theorem in a manner similar to that described by Dawes (1992). Integration in time is accomplished by means of a four step Jameson-style Runge–Kutta scheme. Standard boundary conditions are applied (as

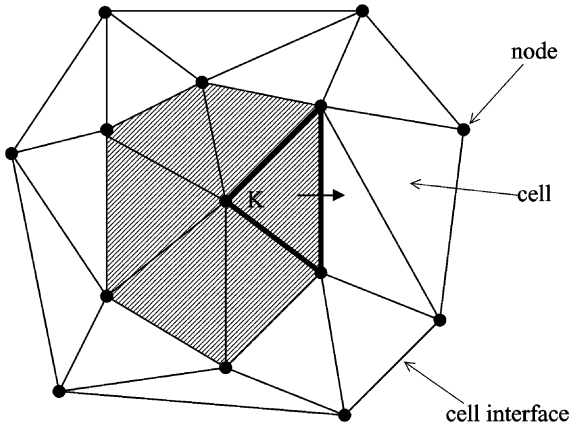

Fig. 1. Control volume on the triangular unstructured mesh. The shaded region shows the control volume associated with the central node, K.

described by Dawes, 1992), and all solid walls are treated as adiabatic.

3.1. Artificial dissipation

As with all Jameson-style schemes, artificial dissipation terms are required to dampen oscillations in the vicinity of flow discontinuities, and to prevent odd–even decoupling. An adaptive blend of Laplacian and biharmonic terms are added, in the fashion described by Mavriplis and Jameson (1987). However, in regions of rapidly nucleating flow, low-order moments of the droplet size distribution behave in a quasi-discontinuous fashion. The Laplacian dissipation terms for the moment equations are thus added in proportion to an adaptive switch based on the zeroth moment:

$$v_k = \left| \sum_{j=1}^{N} \{(\mu_0)_j - (\mu_0)_K\} \right| \Big/ \sum_{j=1}^{N} \{(\mu_0)_j + (\mu_0)_K\}, \qquad (10)$$

where the summation is carried out for all nodes connected to K by a cell interface (hence, $N = 6$ in the example of Fig. 1).

3.2. Equation of state

Accurate calculations for steam require a real gas equation of state to represent the vapour phase. However, most real gas equations are formulated with either p and T_v or ρ_v and T_v as the independent variables, whereas solution of the conservation equations effectively yields values for the vapour density and internal energy. Following Hill et al. (2000), a look-up table approach has been adopted, whereby values of p and T_v together with the relevant first derivatives ($\partial p/\partial \rho_v$, $\partial p/\partial e_v$, etc.) are stored as functions of ρ_v and e_v. Typically a grid of 30×30 points is used, from which central difference approximations to second derivatives (e.g., $\partial^2 p/\partial \rho_v^2$) are formed. This permits pressure and vapour temperature to be unwrapped from specified values of ρ_v and e_v, using functions that are piecewise quadratic in these two variables. The look-up table may be constructed from any appropriate equation of state; that used here was devised by Young (1992) and is based on the relation

$$p = \rho_v R_v T_v (1 + Z\{p, T_v\}), \qquad (11)$$

where R_v is the specific gas constant for steam and $Z\{p, T_v\}$ is a compressibility parameter. Full details of this equation of state are reported in the paper by Young.

This method requires negligible additional computation relative to dry perfect gas calculations (irrespective of the sophistication of the equation of state used), and yields results that are numerically indistinguishable from those obtained by iterative solution to the full real gas equations.

4. Results for steady condensation in nozzles

Young (1982) has compared measured pressure distributions and droplet sizes with one-dimensional calculations for a wide range of nozzles in an attempt to validate and "tune" the expressions for nucleation and droplet growth. It is not the intention to repeat such an extensive comparison here. Nonetheless, it is of interest to re-compute some of the nozzle flows using the current two-dimensional viscous flow method, since some of the nozzle geometries exhibit significant two-dimensional effects, and these are likely to be modified by boundary layer growth. To some extent, such effects can be accounted for in one-dimensional calculations by inferring the effective nozzle area variation from dry-expansion pressure measurements, but it is conceivable that the viscous effects will be modified when condensation is occurring. Unfortunately, none of the experimental data available in the literature contain sufficient detail of boundary layers (e.g., thicknesses and velocity profiles at nozzle inlet) to fully specify viscous flow calculations. For the purposes of comparison, inviscid, laminar and turbulent calculations are, therefore, presented and boundary layers are allowed to grow from zero thickness at inlet to the computational domain. (Calculations undertaken with different lengths of inlet section show relatively little difference due to the rapid acceleration prior to the throat.) No transition model is included, so where appropriate the boundary layer is assumed turbulent from the inlet.

Fig. 2 shows a typical unstructured mesh (subsequent to adaptive refinement) used for calculations presented below. The mesh is densely packed near the wall to resolve the boundary layer, and has been refined on the basis of changes in the zeroth moment (proportional to the number of droplets per unit mass of mixture) which varies rapidly in the nucleation zone and across the boundary layer. To obtain mesh-independent solutions, it was found that an additional region of refinement was required (selected on the basis of pressure variation) to resolve rapid changes in flow properties just downstream of the throat.

Predictions of nozzle centreline pressure and droplet size are compared in Fig. 3 with experiment for nozzles B and C of Moore et al. (1973). The geometry of these nozzles (given in the reference, and outlined in Appendix C) comprises a circular arc near the throat blended with a straight line section downstream. This discontinuity in curvature produces strong two-dimensional effects, which show up as undulations in the centreline pressure. These are particularly evident in the inviscid calculations, but are smoothed out by growth of the boundary layer in the viscous cases. Substantial differences are also apparent in the computed droplet sizes, and these stem from interference between the pressure undulations and the nucleation zone. It is clear that any tuning of the

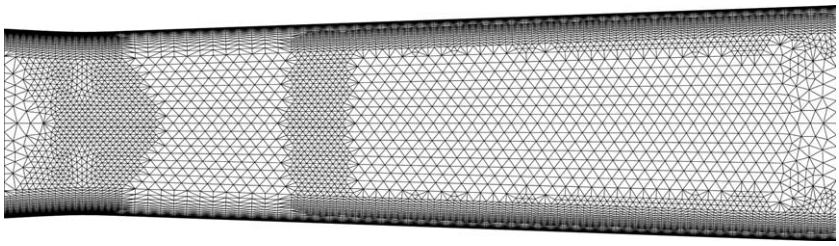

Fig. 2. Refined mesh used for nozzle C (Moore et al., 1973) calculations. Remeshing has been carried out on the basis of pressure variation (upstream region) and zeroth moment (downstream).

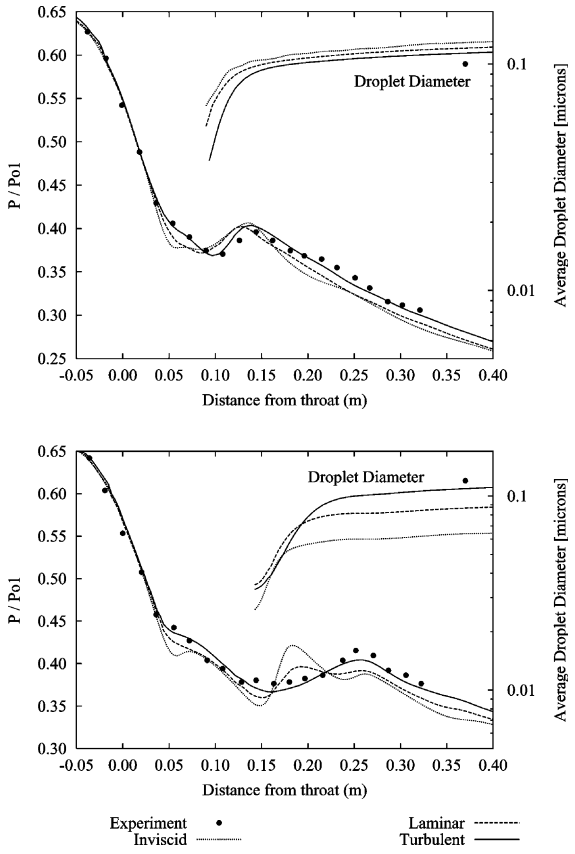

Fig. 3. Comparison of centreline pressure and Sauter mean droplet size with the experiments of Moore et al. (1973): nozzle B (above) computed with $v = 0.54$ and $\xi = 0.4$; nozzle C (below) computed with $v = 0.44$ and $\xi = 0.4$. Turbulent calculations are with an inlet turbulence intensity of 1%, and $\mu_T/\mu_L = 100$.

nucleation and droplet growth equations (for example, via the parameters v and ξ discussed briefly in Appendix B) will depend on how viscous effects are accounted for. For both nozzles, best agreement with experiment is obtained with turbulent calculations, but it must be borne in mind that two-dimensional calculations cannot reproduce the complete effects of boundary layer growth since this also occurs on the nozzle endwalls.

The compressible displacement and momentum thicknesses for turbulent calculations in nozzle C are compared with the corresponding dry flow values in Fig. 4. As expected, the rise in pressure that accompanies the condensation process causes an increase in the momentum thickness. By contrast, the displacement thickness actually reduces slightly in the condensation zone compared with its dry value. This latter effect has also been observed by Schnerr et al. (1992) and is explicable in terms of condensation induced density changes. These minor changes in boundary layer growth have implications for the one-dimensional "effective area" technique discussed above, and indeed none of the pressure distributions computed by Young (1982) agree well with experiment downstream of the condensation zone. The differences are, however, slight and since changes in the boundary layer only occur downstream of the nucleation zone, predicted droplet sizes are unlikely to be affected.

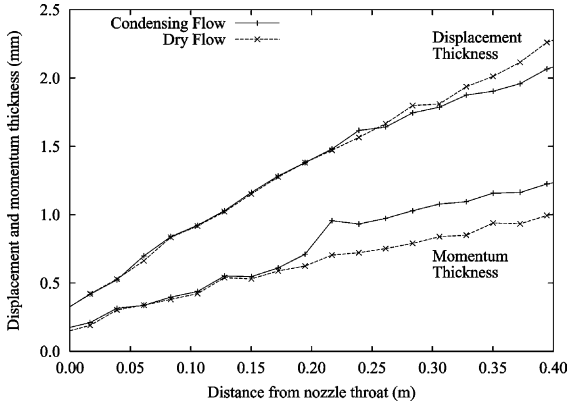

Fig. 4. Compressible displacement and momentum thickness for nozzle C (Moore et al., 1973), computed for dry turbulent flow and condensing turbulent flow.

5. Results for unsteady condensation in nozzles

It is well known that when condensation takes place at near-sonic conditions, periodically unsteady phenomena may result from interaction between the condensation-induced supercritical shockwave and the nucleation zone. Self-excited oscillations of this nature were first discovered for moist air flow by Schmidt (1962), and experimental studies were subsequently

conducted for wet steam by Barschdorff (1971). Since then, a number of numerical results for unsteady condensation have been presented, including the one-dimensional calculations of Skillings and Jackson (1987), and the two-dimensional calculations of White and Young (1993). More recently, however, Adam and Schnerr (1997) have identified a new, asymmetric mode of oscillation for moist air flow, despite their nozzle geometries being perfectly symmetric. This interesting mode comprises a complex pattern of oblique shock-waves, and was first observed experimentally in supersonic nozzles with high inlet relative humidity. Adam and Schnerr were also able to simulate this mode with inviscid flow computations, obtaining excellent agreement for the variation of oscillation frequency with relative humidity. An explanation of why this mode should occur has not yet been published.

In order to ascertain whether such asymmetric oscillations would occur in wet-steam flow, preliminary calculations have been carried out for a range of nozzle geometries, in each case varying both inlet stagnation pressure and temperature. Following the approach of Adam and Schnerr (and in the interests of computational speed), the calculations have been restricted to inviscid flow, using grids of moderate mesh density (typically 1900 computational nodes). The geometries tested so far include nozzles A–E of Moore et al. (1973), and circular arc geometries with various expansion rates. Nozzle E, which has the slowest expansion rate and shows pronounced two-dimensional effects, is the only one as yet to exhibit the asymmetric mode, and only then at inlet pressures of around 1 bar. Contours of $\partial\rho/\partial x$ (equivalent to a Schlieren image) and log nucleation rate are shown in Fig. 5. No adaptive refinement

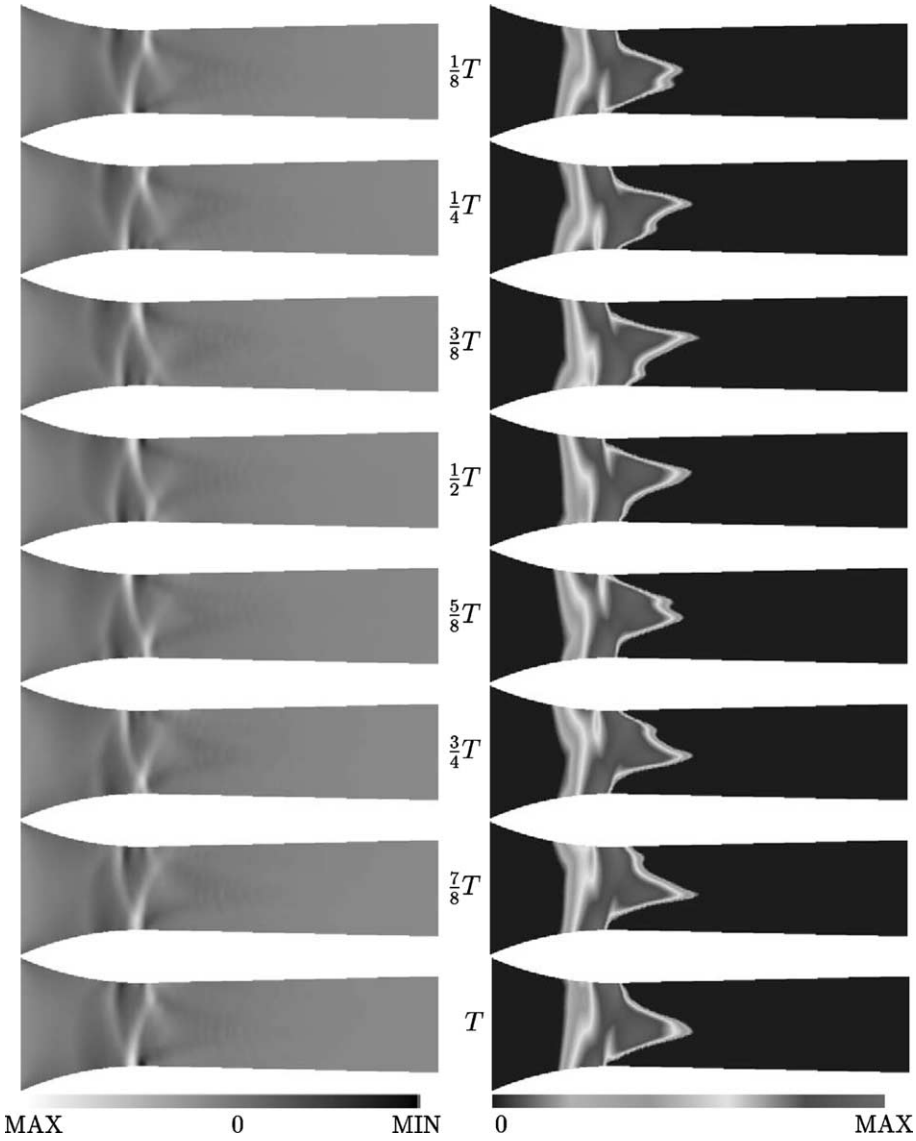

Fig. 5. Contours of $\partial\rho/\partial x$ (left) and $\log(J)$ (right) for one period of asymmetric oscillation. The geometry is nozzle E (Moore et al., 1973), with inlet conditions of $P_{01} = 1$ bar and $T_{01} = 372$ K. (T is the time for one period oscillation.)

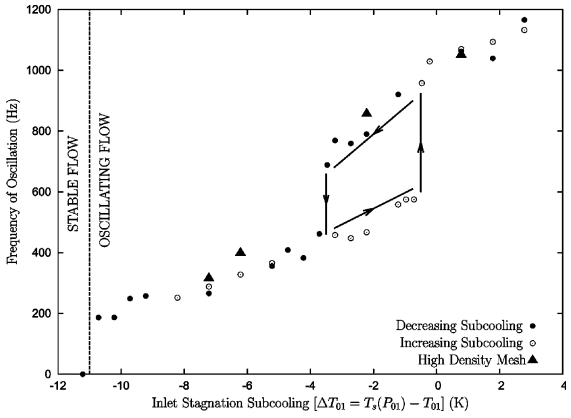

Fig. 6. Dependence of oscillation frequency on inlet subcooling for nozzle E (Moore et al., 1973), with $P_{01} = 1$ bar. Two oscillation modes are possible for inlet subcooling in the range −3.8 K to −0.25 K (i.e., slightly superheated inflow). Standard mesh ≈1900 nodes, fine mesh ≈17 K nodes.

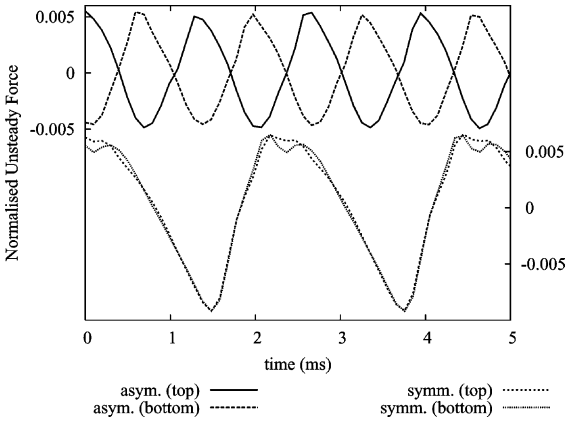

Fig. 7. Unsteady force components on the nozzle top and bottom walls. The geometry is nozzle E (Moore et al., 1973) with $P_{01} = 1$ bar and $T_{01} = 375$ K. Note that for the symmetric oscillations, the top and bottom wall forces are not identical due to slight asymmetry in the mesh.

has been applied, so the shock waves are rather smeared. Nonetheless, the same sequence of oblique shock structures as observed in the experiments of Adam and Schnerr is clearly discernable. The log nucleation contours are included chiefly for comparison with the paper of Adam and Schnerr, but these also clearly demonstrate the periodic asymmetry and mutual influence of phase change and the oblique shock structure.

That these results are not merely a facet of the numerical scheme is evident from Fig. 6, which depicts the variation of oscillation frequency with decreasing inlet stagnation temperature (plotted as inlet stagnation subcooling in the figure). As the inlet temperature is reduced (equivalent to increasing inlet relative humidity for moist air flow), the flow pattern passes first through steady supercritical and then symmetric unsteady supercritical regimes. The frequency of the symmetric oscillations increases with reduction in temperature, but there is a limit below which this mode can no longer be sustained. The frequency then jumps by a factor of approximately 2, indicating the onset of the asymmetric mode. If calculations are then continued whilst gradually increasing the temperature, an upper temperature limit (or lower limit in subcooling) is reached, above which the oscillations revert to the lower frequency, symmetric form. These features, including the frequency hysteresis, were computed by Adam and Schnerr using a very different numerical scheme, and there is no doubt that they constitute genuine flow phenomena. (Fig. 6 also shows a few results computed with a fine mesh [approximately 17 K nodes], and these indicate no strong dependence on mesh density.)

Although the asymmetric oscillation mode has also been predicted within asymmetric geometries for moist air flow (Heiler, 1999), there is as yet no evidence to suggest that it will occur within the highly asymmetric blade passages of steam turbines. However, if it were to do so, it may have implications for both aerodynamic performance and blade flutter. In this respect, Adam and Schnerr (1997) predicted substantially larger amplitude pressure oscillations for some of the asymmetric cases than for the symmetric mode. The unsteady force component,

$$f = \int_{\text{inlet}}^{\text{outlet}} (p - \bar{p}) \mathrm{d}x \tag{12}$$

(where $\bar{p}$ is the time-averaged pressure), normalised with respect to the steady component, is plotted in Fig. 7 for the upper and lower walls, and for both the symmetric and asymmetric oscillation modes. For this particular nozzle, the amplitude of the oscillatory force is slightly greater for the symmetric mode, which is in contrast to the results presented by Adam and Schnerr for the variation of pressure at their nozzle's throat. However, the magnitude of such unsteady forces is likely to depend on nozzle geometry, and further study with other nozzle profiles is required before general conclusions can be drawn.

6. Conclusions

A calculation method for viscous flow of condensing steam has been presented, together with results for steady and unsteady flow in nozzles. The method employs unstructured grids which may be adapted in the rapidly changing condensation zone. Viscous calculations for steady flow indicate that growth of the boundary layer has a significant impact on the predicted pressure distributions and droplet sizes, at least for cases where two-dimensional effects are prominent.

Unsteady, inviscid calculations for a variety of nozzle geometries have revealed that asymmetric modes of

oscillation, which have previously only been observed in moist air flow, may also occur in steam. So far, these have been found for just one nozzle geometry and further investigation is required to ascertain under what circumstances the asymmetric modes occur.

Appendix A. Parameters and constants for the turbulence model

The turbulence model given in Eqs. (4)–(6) is particularly suited to capturing near wall turbulence. The damping term, f_μ, included in Eq. (4) accounts for wall effects and is given by

$$f_\mu = \sqrt{1 - \exp(-a_1 Re_\eta - a_3 Re_\eta^3 - a_5 Re_\eta^5)}, \tag{A.1}$$

where Re_η is the turbulent Reynolds number,

$$Re_\eta = \frac{\rho\eta\sqrt{k}}{\mu_L}. \tag{A.2}$$

η being the normal distance to the nearest wall. The constants a_1, a_3, a_5 are equal to 1.5×10^{-4}, 5×10^{-7} and 1×10^{-10}, respectively.

The turbulent time scale, t_T, (Eq. 6) is given by summation of the conventional turbulent time scale and the Kolmogorov time scale,

$$t_T = \frac{k}{\varepsilon} + \sqrt{\frac{\mu_L}{\rho\varepsilon}}. \tag{A.3}$$

The first term dominates far from the wall, but tends to zero close to the wall since a zero k wall boundary condition is imposed.

The remaining constants C_μ, $C_{\varepsilon1}$, $C_{\varepsilon2}$, σ_k, σ_ε in Eqs. (4)–(6) take the values 0.09, 1.44, 1.92, 1.0 and 1.3, respectively.

Appendix B. Droplet growth and nucleation

The droplet growth expression adopted for the current work is a slightly modified version of the standard Gyarmathy equation:

$$G(r) = \frac{dr}{dt} = \frac{\lambda_L \Delta T(1 - r_*/r)}{\rho_l(h_v - h_l)(r + 1.89(1-v)l_v/Pr)}. \tag{B.1}$$

The factor $(1 - v)$ is a semi-empirical correction introduced by Young (1982) to obtain agreement with experimental data for low-pressure nozzle expansions. The form of v is given in White and Young (1993). Although this correction may be justified on physical grounds (if the condensation and evaporation coefficients were to differ under non-equilibrium conditions), v is effectively a tunable constant, and the values required to give agreement with experiment are given in the relevant figure captions. The average growth rate, $\overline{G}$, used in Eq. (9) is approximated by evaluating $G(r)$ at the local Sauter mean radius, $r_{32} = \mu_3/\mu_2$. This is the only approximation involved in Eq. (9), and only incurs significant error for very broad size distributions, (see White, 2003).

Note that Eq. (B.1) includes the dependence of droplet temperature on radius through the term r_*/r. This term accounts for droplet capillary subcooling and is significant only for very small droplets. The critical radius, r_*, is defined by:

$$r_* = \frac{2\sigma T_s}{\rho_l(h_v - h_l)\Delta T}. \tag{B.2}$$

The nucleation rate is calculated from classical theory, modified to include non-isothermal effects Kantrowitz (1951):

$$J_{CL} = \frac{q_c}{1+\Phi}\left(\frac{2\sigma}{\pi M^3}\right)^{\frac{1}{2}}\frac{\rho_g}{\rho_l}\exp\left(-\frac{4\pi r_*^2\sigma}{3kT_g}\right), \tag{B.3}$$

where q_c is the condensation coefficient (assumed equal to unity), and $(1 + \Phi)$ is the non-isothermal correction factor. The definition of Φ is standard and can be found with discussion in Young (1982). Calculations undertaken for a range of nozzle experiments (Simpson, 2004) indicate that droplet sizes are consistently underpredicted when using Eq. (B.3). Accordingly, a correction is applied to J_{CL} such that the nucleation rate used in Eq. (9) is,

$$J = \xi J_{CL}, \tag{B.4}$$

with values for ξ typically $\sim$0.4. It is somewhat unsatisfactory that such an adjustment should be necessary, but it is worth pointing out that the required reduction in nucleation rate could be achieved by a less than 2% increase in surface tension. (The value of σ is assumed independent of droplet radius in Eqs. (B.2) and (B.3).)

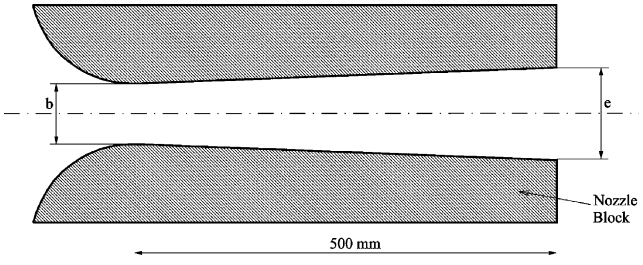

Nozzle	B	C	E
b (mm)	100	120	140
e (mm)	144	150	157

Fig. 8. Geometry of the rectangular Laval nozzles. (The depth of the experimental test section was 152 mm.)

Appendix C. Details of the nozzle geometry

The nozzles were formed from two shaped blocks placed between parallel sidewalls. The blocks were rotated and positioned to give the geometries outlined in Fig. 8, (fuller details are given in Moore et al., 1973). The nozzles B, C and E produce progressively decreasing rates of expansion typical of flows though turbine blade rows.

References

Adam, S., Schnerr, G.H., 1997. Instabilities and bifurcation of non-equilibrium two-phase flows. J. Fluid Mech. 348, 1–28.

Barschdorff, D., 1971. Variation of the variables of state and gas-dynamical relationships during the spontaneous condensation of pure steam in Laval nozzles. Forsch. Ing. Wes. 37, 146–157, translated by the National Translations Center.

Binnie, A.M., Woods, M.W., 1938. The pressure distribution in a convergent–divergent steam nozzle. Proc. Inst. Mech. Eng. 138, 229–266.

Dawes, W.N., 1992. The practical application of solution-adaption to the numerical simulation of complex turbomachinery problems. Prog. Aerosp. Sci. 29, 221–269.

Heiler, M., 1999. Instationäre Phänomene in homogen/heterogen kondensierenden Düsen- und Turbinenströmungen. Ph.D. thesis, Karlsruhe.

Hill, P.G., 1966. Condensation of water vapour during supersonic expansion in nozzles. J. Fluid Mech. 25 (3), 593–620.

Hill, P.G., Miyagawa, K., Denton, J.D., 2000. Fast and accurate inclusion of steam properties in two- and three-dimensional steam turbine flow calculations. Proc. Inst. Mech. Eng. 214 (Part C), 903–919.

Kantrowitz, A., 1951. Nucleation in very rapid vapour expansions. J. Chem. Phys. 19 (9), 1097–1100.

Mavriplis, D., Jameson, A., 1987. Multigrid solution of the two-dimensional Euler equations on unstructured triangular meshes. In: AIAA 25th Aerospace Science Meeting, Reno, Nevada, January 12–15, 1987. AIAA-87-0353.

Moore, M.J., Walters, P.T., Crane, R.I., Davidson, B.J., 1973. Predicting the fog-drop size in wet-steam turbines. In: Institute of Mechanical Engineers Conference Publication, Wet Steam 4, Warwick. pp. 101–109. C37/73.

Schmidt, B., 1962. Beobachtungen über das Verhalten der durch Wasserdampf-kondensation ausgelösten Störungen in einer Überschall-Windkanalduse. PhD thesis, Fakultät für Maschinenbau, Universität Karlsruhe, Deutschland.

Schnerr, G.H., Bohning, R., Breitling, T., Jantzen, H.A., 1992. Compressible turbulent boundary layers with heat addition by homogeneous condensation. AIAA J. 30 (5), 1284–1289.

Simpson, D.A., 2004. Numerical modelling of condensing wet-steam flows. Ph.D. thesis. Cambridge University Engineering Department.

Skillings, S.A., Jackson, R., 1987. A robust 'time-marching' solver for one-dimensional nucleating steam flows. Int. J. Heat Fluid Flow 8 (2), 139–143.

Stodola, A., 1905. Steam Turbines: with an Appendix on Gas Turbines and the Future of Heat Engines. New York. pp. 52–85 (Chapters 16–24, translated from second German edition).

White, A.J., 2000. Numerical investigation of condensing steam flow in boundary layers. Int. J. Heat Fluid Flow 21, 727–734.

White, A.J., 2003. A comparison of modelling methods for polydispersed wet-steam flow. Int. J. Numer. Methods Eng. 57, 819–834.

White, A.J., Hounslow, M.J., 2000. Modelling droplet size distributions in polydispersed wet-steam flows. Int. J. Heat Mass Transf. 43 (11), 1873–1884.

White, A.J., Young, J.B., 1993. Time-marching method for the prediction of two-dimensional, unsteady flows of condensing steam. J. Propul. Power 9 (4), 579–587.

Yang, Z., Shih, T.H., 1993. New time scale based k–ε model for near-wall turbulence. AIAA J. 31 (7), 1191–1197.

Young, J.B., 1982. The spontaneous condensation of steam in supersonic nozzles. Physico Chemical Hydrodynamics 3 (1), 57–82.

Young, J.B., 1992. Two-dimensional, nonequilibrium wet-steam calculations for nozzles and turbine cascades. J. Turbo 114 (July), 569–579.